Shenzi OBN: An imaging step change

Cheryl Mifflin[1], Drew Eddy[1], Brad Wray[2], Lin Zheng[2], Nicolas Chazalnoel[2], and Rongxin Huang[2]

https://doi.org/10.1190/tle40050348.1

Abstract

The story of seismic imaging over BHP's Shenzi Gulf of Mexico production field follows the history of offshore seismic imaging, from 2D to 3D narrow-azimuth streamer acquisition and to its leading the wide-azimuth movement with the Shenzi rich-azimuth (RAZ) survey. Each RAZ reprocessing project over the last 15 years applied the latest processing technology, culminating in hundreds of scenario tests to refine the salt model, but eventually the RAZ data reached a technical limit. A new ocean-bottom-node (OBN) survey acquired in 2020 has produced a step-change improvement over the legacy RAZ image. The uplift can be attributed to several factors. First, an OBN feasibility and survey design study demonstrated that a core of dense nodes combined with sparse nodes would improve the accuracy and resolution of the full-waveform inversion (FWI) solution. Second, the OBN data acquired following the survey design and employing FWI as the main model-building tool realized the predicted improvement. The result was a substantial change to the complex salt model, verified by a salt proximity survey as well as other salt markers, and improvement in imaging over the entire field. In addition to the improvement arising from a more accurate FWI velocity model, the steep-dip imaging also benefited from the new full-azimuth and long-offset data. However, the best steep-dip and fault imaging comes from the FWI image, a direct estimation of reflectivity from the FWI velocity. As the maximum frequency used by FWI moves toward the maximum frequency of the final reverse time migration (RTM), the FWI image approaches the resolution necessary to compete as the primary interpretation volume. Its subsalt illumination surpassed that of the RTM and even the least-squares RTM volumes. These imaging improvements are providing a new understanding of the faults and stratigraphic relationships of the field.

Introduction

Shenzi Field in the Atwater fold belt of the deepwater Gulf of Mexico is a set of subsalt Miocene reservoirs below a thick and complex salt canopy. The field has been producing oil since 2009. The Shenzi-1 discovery well was drilled in 2002 to a depth of 26,607 ft. The production field currently has more than 30 wells and produces 45,000 barrels of oil per day.

Shenzi has a long history of seismic imaging, from 2D in the 1990s and 3D narrow azimuth in the early 2000s to the Shenzi rich-azimuth (RAZ) survey (Howard, 2007), an almost full-azimuth survey acquired in 2005 that was the first multi-wide-azimuth survey in the industry. The RAZ data have since been processed several times, with each reprocessing taking advantage of the latest technology to further improve the imaging. In 2014, the last time the RAZ data were reprocessed, the subsalt image coherence improved significantly over the first RAZ processing, and it appeared to resolve most of the subsalt imaging challenges. However, a zone of poor imaging persisted, primarily around the salt stock. This zone shrank with each successive reprocessing effort, but it remained considerable in size. In particular, poor image quality on the east side of the field made well planning difficult. Fault interpretation was problematic due to challenges in distinguishing complex geology from noise. The amplitudes were also not consistent across reservoir events, indicating possible illumination gaps or an incorrect model. Overall, the subsalt resolution was inadequate for the detailed interpretation needed. It was determined that the RAZ data had reached a technical limit, and additional reprocessing likely would yield only small incremental benefits rather than the major uplift needed to continue optimal field production and identify new opportunities. Due to recent successes with full-waveform inversion (FWI) using long-offset ocean-bottom-node (OBN) data (Michell et al., 2017; Shen et al., 2018; Zhang et al., 2018; Nolte et al., 2019), a new OBN survey was considered the best way to achieve the required improvement in image quality. A feasibility study was performed to ensure that an OBN survey would address the specific imaging challenges that had been identified. This OBN survey was acquired from late 2019 to early 2020.

The processing project was scoped to include reprocessing of the RAZ data, velocity model building centered on time-lag FWI (Zhang et al., 2018; Wang et al., 2019), and a merge of the RAZ and OBN final reverse time migration (RTM) volumes. The project started before the OBN acquisition was completed. The RAZ reprocessing included FWI, with the aim of generating an improved starting model for the OBN FWI. The migrations of the reprocessed RAZ data were used to evaluate the OBN FWI model in the early iterations. As the OBN FWI used raw data to derive a full velocity model from top to bottom, it was possible to produce a RAZ RTM fast-track volume from an OBN FWI model one month after acquisition completion, early enough to influence the planning of an upcoming well.

Although the Shenzi velocity model had been worked and reworked over many years, the changes resulting from FWI enabled by the OBN data were substantial. This paper will review the major components of the survey design, velocity model building, and imaging that contributed to the step change in subsalt image quality. We also describe the impact that the new OBN imaging has made on the interpretation.

[1]BHP, Houston, Texas, USA. E-mail: cheryl.mifflin@bhp.com; drew.eddy@bhp.com.
[2]CGG, Houston, Texas, USA. E-mail: brad.wray@cgg.com; linn.zheng@cgg.com; nicolas.chazalnoel@cgg.com; rongxin.huang@cgg.com.

Feasibility and survey design

Understanding the imaging challenges was key to demonstrating that a new OBN survey would be able to resolve them. To that end, synthetic data were generated from a detailed 3D synthetic model in order to analyze the imaging issues and design an OBN survey with optimal parameters.

The density model was built in SKUA-GOCAD using several layers, including salt and reservoir horizons. Twenty-seven density well logs were propagated within the layers. Faults were inserted manually to ensure that sharp discontinuities were included in the model (Figure 1). Once the finite-difference data were generated, noise and multiples from the real RAZ data were added to the synthetic RAZ data. However, even with this noise inserted, the RTM image of the actual RAZ data was still much noisier and less coherent than the image of the synthetic data. To simulate the effect of an incorrect model, changes were made to the true model. Sediment inclusions were removed in the salt, and the top of salt (TOS) was smoothed. After these changes, the migration image of the synthetic data approached the degraded subsalt image observed with the RAZ data. This indicated that velocity error was likely the main reason for the poor subsalt image in the real data. With an inaccurate velocity model identified as the primary cause for poor subsalt imaging and FWI as the best hope to improve it, the focus shifted to determining the OBN survey parameters needed to optimize the FWI outcome.

Acquisition parameters were selected based on tests using the synthetic data set while taking into account cost considerations. The node footprint was chosen based on node contribution maps for a number of key subsalt horizons (van Gestel et al., 2015; Chakraborty et al., 2017). These maps show the relative contribution of each node to the amplitude of the migrated image on selected target horizons using a normalized root-mean-square measurement (Figure 2a). Migration and FWI checkerboard inversion tests were used to determine the other main acquisition parameters, such as shot halo, crossline offset, shooting direction, blending noise effect, and node sampling. Although 200 × 200 m node sampling gave the best imaging results, the chosen node sampling was 400 × 400 m due to the availability of nodes and because the RAZ offered a relatively good complement to the OBN. In addition, the study showed that there would be significant FWI resolution improvement from placing sparse nodes at a 1 × 1 km spacing within a 10 km halo around the core dense-node footprint, which led to the final design in Figure 2b. This decision proved to be wise, as the sparse nodes ended up being critical to the success of the project.

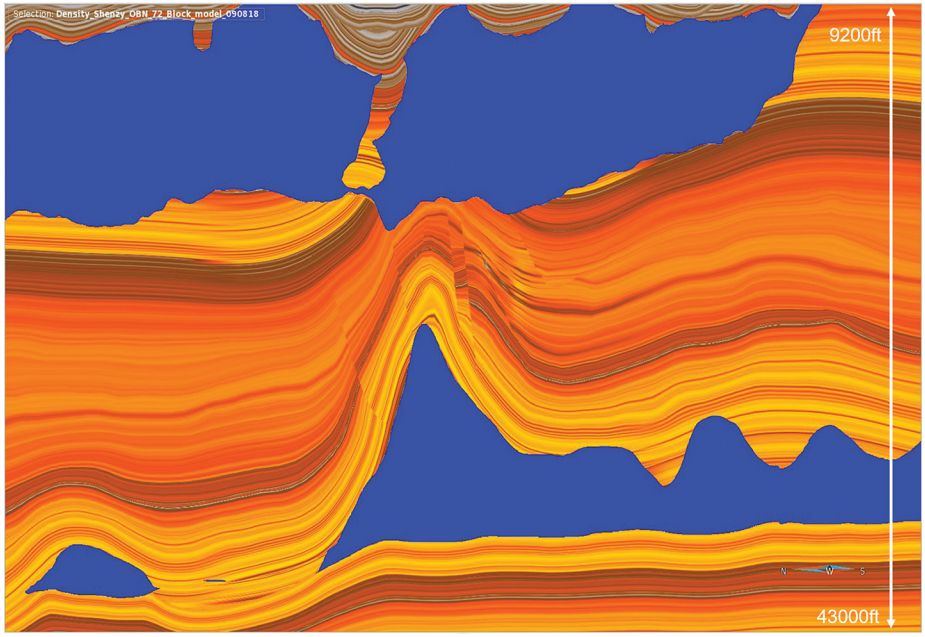

Figure 1. The density model used for synthetic generation was built with information from density logs propagated along the layers. Faults were inserted manually into the model.

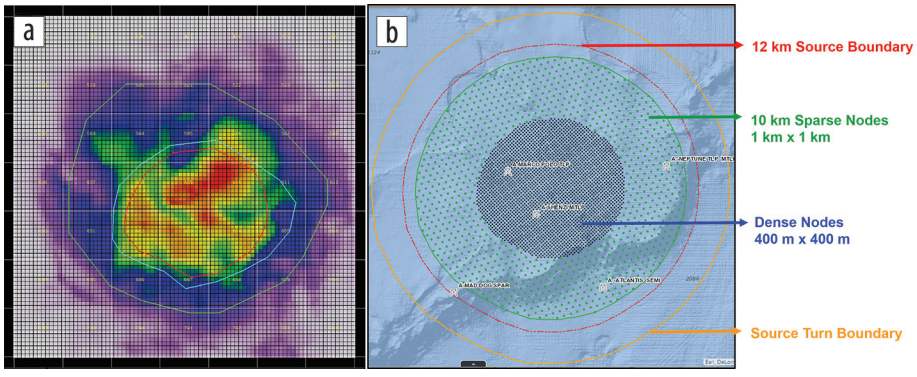

Figure 2. (a) A node hit map from the feasibility study on a target horizon. Warm colors indicate higher contribution of the node location to the target horizon. The red and cyan polygons represent smaller and larger target areas, respectively. The green polygon shows the optimal dense-node coverage. The OBN node and source layouts are shown in (b). The feasibility study recommended a dense core of approximately 2500 nodes for imaging and model building and an outer ring of approximately 1000 sparse nodes to further aid FWI in resolving the complexity of the velocity field. The sparse node ring extends 10 km outside of the dense-node core, and the shot halo extends an additional 2 km beyond the sparse node boundary.

FWI for velocity update

The velocity model building commenced with the existing RAZ data while the OBN acquisition was ongoing, with the goal of improving the input model for the OBN FWI. Beginning from a smoothed version of the legacy velocity model, three rounds of RAZ FWI with frequencies up to 6 Hz were run. Each time, edits were made to the initial model based on well information, subsalt velocity updates from RTM surface offset gathers, or modifications

to the salt as indicated by the changes made in the previous round of FWI (Kumar et al., 2019).

Figures 3a–3d show the legacy and third-round RAZ FWI models and their corresponding 15 Hz RAZ RTM images. These initial rounds of RAZ FWI produced a clear improvement in imaging over legacy results, increasing event continuity and coherency. The salt feeder was reshaped, widening in the shallow section, with indications of faster velocities in the Mesozoic packages observed at the bottom of the subsalt basins, and climbing along the feeder flank. The deep autochthonous base of salt (BOS) and basement events began to flatten and come into focus, indicating an improved velocity above.

While the RAZ FWI updates delivered good uplift to the image and gave some indication of the potential improvement to come from OBN FWI, the 8.5 km maximum offset of the streamer data set limited the ability of FWI to update the deeper section of the model. Here, the inversion is driven almost entirely by reflection energy, and the update is not able to move far enough from the starting model (Figure 3b). To better resolve the velocity in the deeper section, the OBN data with their clean low-frequency signal and substantially longer offsets were needed.

By the time the OBN acquisition ended, the starting velocity model was ready. Maximum offsets for the OBN data range from approximately 20 to 45 km, depending on the location of the node within the survey area. A good signal-to-noise ratio (S/N) at low frequency combined with the advanced time-lag FWI algorithm enabled the OBN inversion to start at 1.6 Hz, reducing the chance of cycle skipping. The maximum frequency of the OBN inversion was 11 Hz, and while we did see improvements in focusing and coherency up to the maximum frequency, the bulk of the kinematics was captured by 6–7 Hz.

Figures 3e and 3f show the OBN FWI model and RAZ RTM image for comparison with legacy and RAZ FWI. The OBN FWI further expanded the salt stock and changed details of its shape. It also changed the subsalt velocities essentially everywhere. Most notably, velocities in the Mesozoic sections were increased, with the trend becoming more conformal to the geology. Compared to the RAZ FWI, events are repositioned and more coherent at the reservoir level with the OBN FWI. Basement and deep BOS events continue to flatten, which is another indication of improved kinematics. To reduce turnaround time for a fast-track product, an inversion using only the dense nodes was run to 6 Hz. The production-level inversion started from the same input model but used all nodes (dense and sparse). We compared the 6 Hz models and corresponding RTM images from the fast-track and production inversions to gauge the impact of the sparse nodes on the update. Introducing sparse nodes into the acquisition shot halo is a cost-effective means to increase the node footprint, and even though the S/N of the inverted solution is lower over the sparse node footprint, the resulting RTM image is not significantly different (Mei et al., 2019; Xue et al., 2020). As predicted by the synthetic study, the additional constraints from sparse nodes enable FWI to further resolve the model in the more complex areas. Figure 4 shows the 15 Hz RAZ RTM images migrated with the legacy model, the dense-node-only 6 Hz FWI model, and the all-node 6 Hz FWI model. The inline and crossline pass through the TOS marker of a salt wing protruding from the feeder. This wing was encountered unexpectedly while drilling. The legacy model ties the marker due to manual insertion of the wing, but little information was available for the interpretation aside from the marker position (Figures 4a and 4d). The dense-node-only FWI reshapes the salt geometry, dramatically improving the image, but increases the mis-tie (Figures 4b and 4e). Adding the sparse node data to the inversion further refines the salt geometry in this complex location and greatly reduces the mis-tie (Figures 4c and 4f).

Model accuracy

Even after many years of refining the velocity model over Shenzi Field, FWI still delivered significant broad-brush changes to the salt model and subsalt velocities. While the uplift on the image is clear and subsalt markers match the seismic, the amount of change to the salt geometry naturally raised questions about

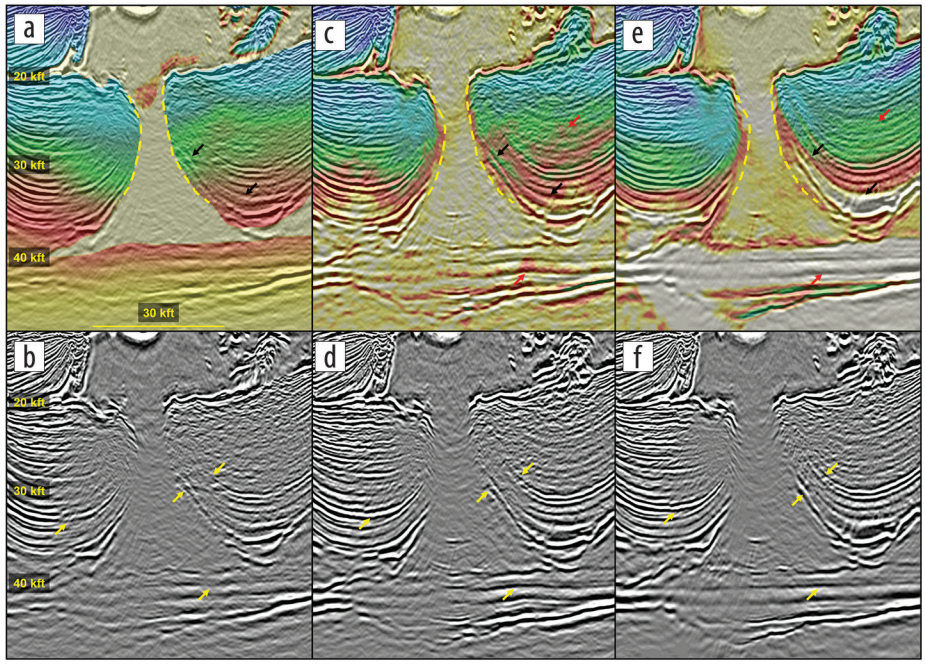

Figure 3. (a) 15 Hz RAZ RTM images migrated with the legacy model, (c) 6 Hz RAZ FWI model, and (e) 11 Hz OBN FWI model with models overlaid. The same RTM images without models overlaid are shown in (b), (d), and (f). The dashed yellow lines show the extent of the legacy salt feeder, which was expanded by RAZ FWI and further expanded by OBN FWI. Noise on the RAZ FWI update (red arrows) is not present on the OBN FWI updated model. Faster velocities in the Mesozoic section (black arrows) are detected. RAZ FWI shows some hints, while OBN FWI better defines the high-velocity packages, and the zones can be seen climbing along the feeder flank. The RTM images show improved event coherence and continuity (yellow arrows). The strong basement event begins to flatten and focus after RAZ FWI. With OBN FWI, the focusing and continuity improve further.

the validity of the new model. Evaluation of the model accuracy and FWI convergence was performed through a number of quality-control measures including diving-wave analysis, model comparisons against data from a salt proximity survey, and FWI tests using different initial models.

Diving-wave analysis. Diving-wave illumination maps from large scattering-angle RTM images (Ahmed, 2018) were produced for three different data-model combinations: (1) real data migrated with the OBN FWI input model, (2) real data migrated with the OBN FWI output model, and (3) synthetic data generated and migrated with the OBN FWI output model. These maps give a qualitative picture of the diving-wave illumination in the subsurface and, for the real-data case, the accuracy of the model. The synthetic case represents the ideal situation (true model and high S/N). Because the true model is used to generate and migrate the synthetic data, the forward- and back-propagated wavefields will be in phase along the entire wavepath, and the map can be interpreted as a guide for diving-wave penetration (Figure 5c). In the real-data case, our model is still not completely correct, and the S/N of the data can be poor, especially at very long offsets (greater than approximately 20 km). The large increase in amplitude of the real-data output model illumination map over the input model map indicates a stronger cross-correlation between source and receiver wavefields, implying a more accurate velocity model (Figures 5a and 5b). The real-data output model and synthetic data maps show similar illumination patterns and relative amplitudes, with the deeper subsalt basins and the feeder itself being relatively well illuminated by diving waves and weaker zones of illumination at BOS. Although this is a qualitative technique, it does indicate that the updated model is more accurate and the real-data illumination is approaching the ideal synthetic case.

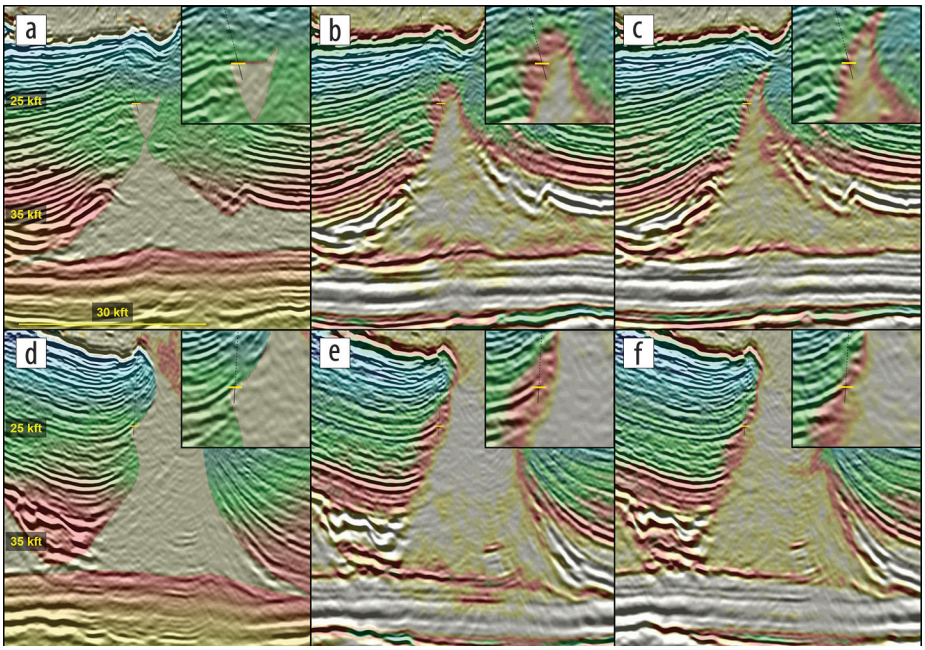

Figure 4. Inline view of 15 Hz RAZ RTM images with velocity model overlaid for (a) legacy, (b) 6 Hz dense-node-only FWI, and (c) 6 Hz all-node FWI taken through the TOS marker for the salt wing (yellow). The crossline view is shown on the bottom row. Zoom-ins are shown in the upper right. (a) and (d) Before FWI, the legacy model matched the salt marker well due to manual interpretation. (b) and (e) After dense-node-only FWI, the shape of the salt is changed dramatically, but the mis-tie becomes worse. (c) and (f) Adding the sparse nodes to the inversion further refines the salt geometry, and the well tie is greatly improved.

Salt proximity survey. As a blind test, a vertical seismic profile salt proximity survey was provided only after the model was derived by the OBN FWI. Figure 6 shows the estimated position of the salt flank compared to different velocity models. The salt flank of the legacy model, built following a

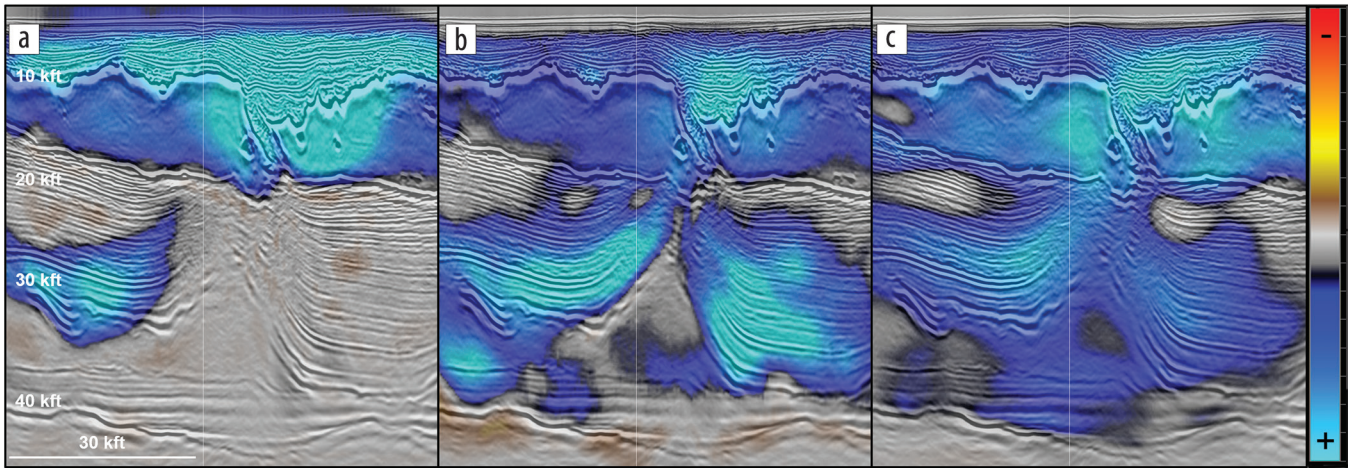

Figure 5. Diving-wave illumination maps for (a) real data migrated with the OBN FWI input model, (b) real data migrated with the OBN FWI output model, and (c) synthetic data generated from and migrated with the OBN FWI output model. Blue shades indicate areas of positive correlation, and browns indicate areas of negative correlation. The amplitude increases significantly after the FWI update, and the illumination along the salt feeder is relatively good. The areas directly beneath BOS have weaker illumination. The map from real data with the FWI output model is consistent with the ideal synthetic case.

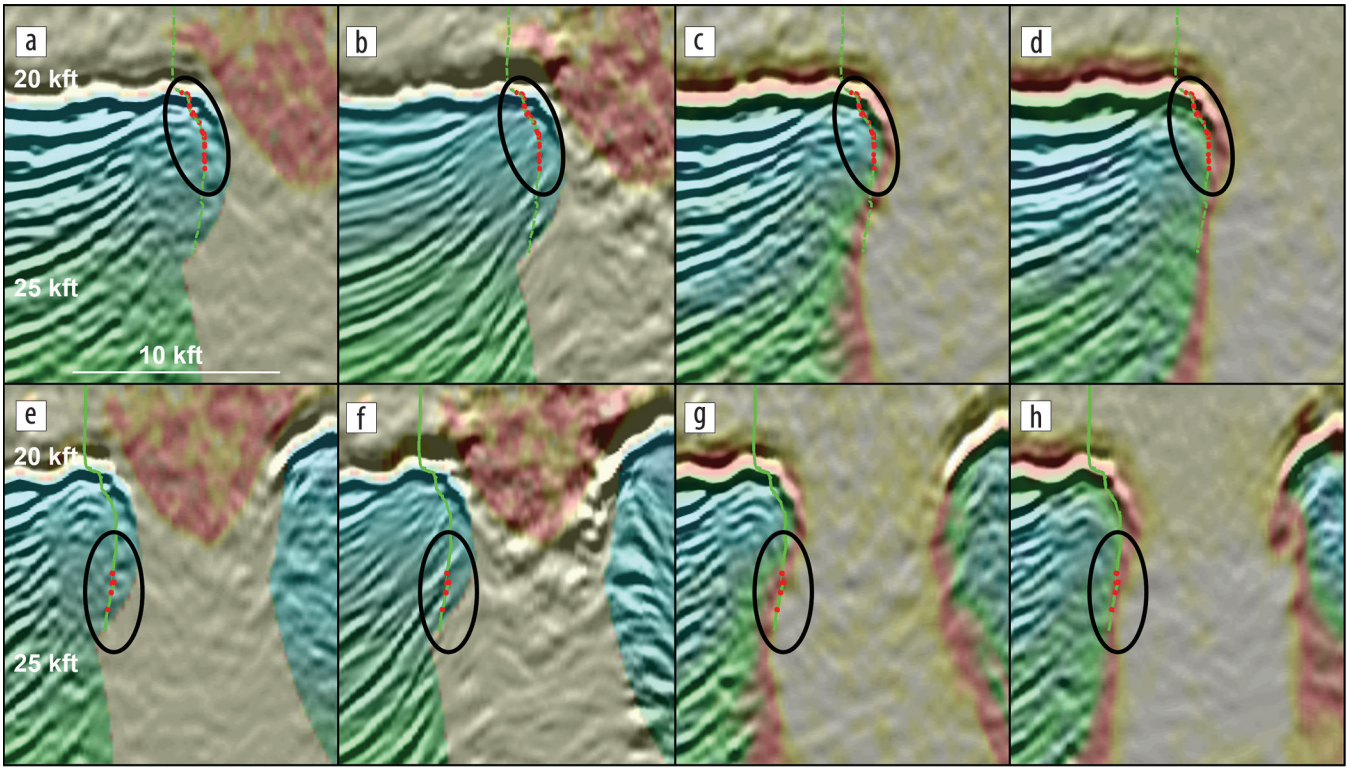

Figure 6. (a) Legacy model overlaid with the corresponding RTM image along the shallow part of the salt interface according to the salt proximity survey. (b) The same legacy model but overlaid on the enhanced legacy stack. (c) and (d) The RAZ FWI and OBN FWI models overlaid on their respective RTM images. (e)–(h) The corresponding deeper sections. The interface is marked by the green lines, and the red dots indicate where the seismic slice intersects the interface estimated by the survey. The legacy model is missing a large amount of salt, and the legacy postmigration enhancement extended some events across the interface estimated from the proximity survey. The RAZ FWI model already starts refining the salt wing but cannot correct the large error in salt geometry. The OBN FWI model shows a very good match with the proximity survey data.

conventional top-down model-building flow with manual interpretation of salt horizons and the best velocity model at the time, is far from the location given by the proximity survey (Figures 6a and 6e). Consequently, selective dip-filtering postmigration enhancement on the legacy image extended some sediment events beyond the estimated salt-flank position, highlighting the danger of such techniques (Figures 6b and 6f). The RAZ FWI already brings the salt flank closer to the salt proximity survey location, but it underestimates the amount of salt in the shallow section and overestimates the amount of deep salt (Figures 6c and 6g). The OBN FWI model gives the best match to the salt proximity data, refining the shape of the salt feeder so it agrees well in the shallow and deep sections (Figures 6d and 6h). The good match of the model, derived by FWI with the salt proximity survey, supports the validity of the large salt increase in the feeder. Although the estimated flank position from the salt proximity survey has its own uncertainty, it is good to see that the two independent approaches arrive at similar conclusions. This quality control also highlights the power of the data-driven FWI workflow to construct accurate velocity models in complex regions where conventional interpretation-based model-building approaches can be severely inadequate.

Starting model. The size of the Shenzi salt feeder increased considerably with OBN FWI, but this had already started with RAZ FWI, making us question whether RAZ FWI put us in a local minimum. To test the convergence of the FWI solution and the corresponding data constraints at this location, another inversion was run, starting directly from the smoothed legacy model. This model has far less salt in the neck of the feeder. The two starting models also had large differences in the deep basin velocities and in the velocities along the salt flank (Figures 7a and 7b). Aside from the difference in starting model, the two inversions were carried out in the same manner (identical starting frequency, maximum frequency, input seismic data, and number of iterations). The output models from the two inversions, shown in Figures 7c and 7d, are quite consistent despite starting from very different points. The amount of salt in the feeder was increased by FWI in both cases and more significantly for the inversion starting from the legacy model. Fast carbonate velocities at the bottom of the basins and along the salt flanks were detected in both cases as well. The two starting models result in images of comparable quality, with some small differences in depths. This indicates the OBN data provide good constraints for FWI to successfully converge.

Imaging

The feasibility study indicated that an inaccurate velocity model was the main reason for poor subsalt image quality, and the updated velocity from OBN FWI greatly improved the image, increasing event coherency and continuity. While this achieved the main goal for acquiring OBN data, there was an expectation from the synthetic study that the subsalt image would also benefit from the additional offset and azimuth coverage. As it turned out, the imaging uplift it provided was significant. Offsets up to

approximately 20 km led to substantial benefits for steep-dip imaging of events along the Shenzi salt stock. Many of these events along the feeder flank could not be imaged at all with the RAZ data, even with a much-improved velocity model, but are now visible on the OBN RTM image (Figures 8a and 8b). The sparse node data, which were acquired to aid the model building, also gave a sizeable contribution to the steep dips along the feeder, albeit with some trade-off in S/N (Figure 8c).

Nevertheless, the RTM image shows that the illumination is still relatively poor in many places, even with OBN data. The image domain single-iteration least-squares RTM (LSRTM), which is based on matching filters in the curvelet domain (Wang et al., 2016) and runs on angle gathers, offers good improvement in these low-illumination zones. A comparison of 15 Hz RTM and LSRTM images is shown in Figures 9a and 9b. Amplitudes of the steeply dipping events along the feeder flank are enhanced by LSRTM. Yet, some events still appear weak or even nonexistent in several locations. The FWI image volume, an approximation of the reflectivity derived directly from the FWI velocity model (Zhang et al., 2020), provides the best compensation and most balanced amplitudes. The FWI image is calculated by taking the derivative of the velocity model along the normal direction to the reflector dips, assuming that the density is constant.

There are some key differences between RTM or LSRTM and the FWI image. First, the input to RTM is the processed downgoing primary reflection energy after free-surface multiple attenuation, while FWI uses raw data containing transmission waves, primary reflection energy (both upgoing and downgoing), and their free-surface and internal multiples. These additional modes can provide increased subsurface illumination, which is critical for imaging in complex areas. Second, the FWI image is derived from the FWI velocity model generated through a least-squares data-fitting process. Therefore, the FWI image exhibits many of the characteristics typical of least-squares migration, including more balanced amplitudes due to compensation of input fold heterogeneity and illumination variations and reduced migration artifacts.

In Figure 9c, the FWI image shows a more balanced amplitude along the poorly illuminated steep dips, similar to LSRTM. The

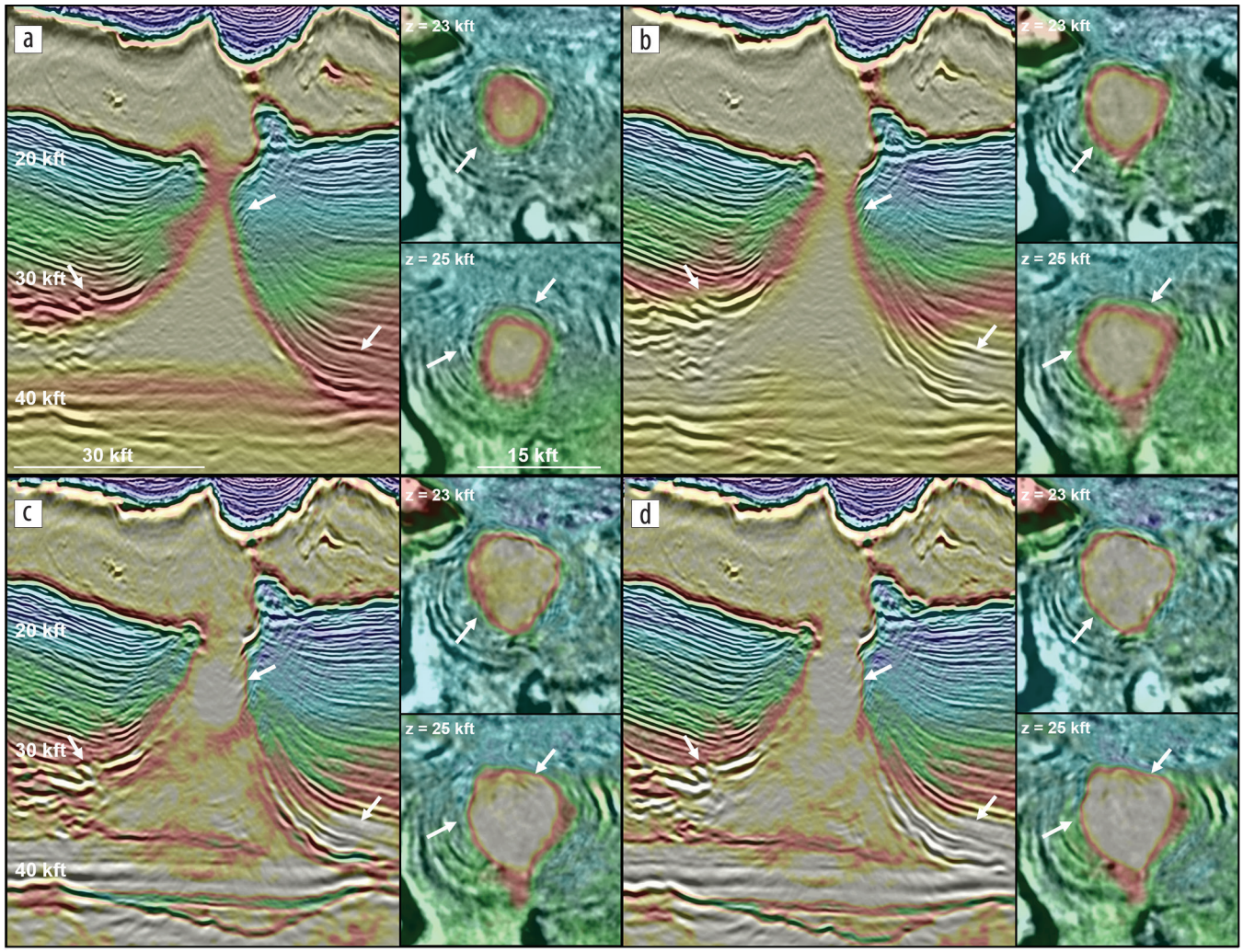

Figure 7. (a) Smoothed legacy model. (b) Smoothed RAZ FWI model. (c) OBN FWI output starting from (a). (d) OBN FWI output starting from (b). Depth slices are shown at 23,000 and 25,000 ft. The salt feeder is much larger on the RAZ FWI model than the legacy model, and the deep basin velocities are quite different between the two starting models. FWI converges to a very similar solution starting from either model with comparable images.

FWI image is superior in the most illumination-challenged areas, such as the shallow subsalt just below BOS. The steep events extend all the way to BOS with relatively strong amplitudes, while they cannot be seen at all on the LSRTM image. It is difficult to know for certain if this region could be illuminated by modes other than downgoing primary reflections. Illumination from nonprimary modes would make it nearly impossible for Born-modeling-based LSRTM to compensate the amplitudes properly. Another point to note is that although the FWI image is not free of noise, its S/N is higher than the raw RTM image and comparable to LSRTM.

The initial scope of the project was to rely on FWI for model building and RTM for imaging, with a planned maximum frequency for FWI of 11 Hz. However, since the FWI image at 11 Hz showed clear imaging benefits over RTM, the decision was made to increase the maximum frequency of the inversion to 20 Hz with the purpose of generating a high-frequency FWI image more comparable to the final 25 Hz RTM volume. Figure 10 compares the 11 and 20 Hz OBN FWI images with the 25 Hz final RTM. At 20 Hz, the resolution of the FWI image is approaching that of the 25 Hz final RTM subsalt, but with higher S/N and more balanced amplitudes. The high-frequency FWI image is particularly good at imaging steep dips and faults. The combination of high resolution, improved illumination, and good S/N make the FWI image a direct competitor to RTM as the primary structural interpretation volume. Note that even though its amplitudes are consistent with those from RTM, they still need to be taken with caution, as a constant density is assumed for its derivation.

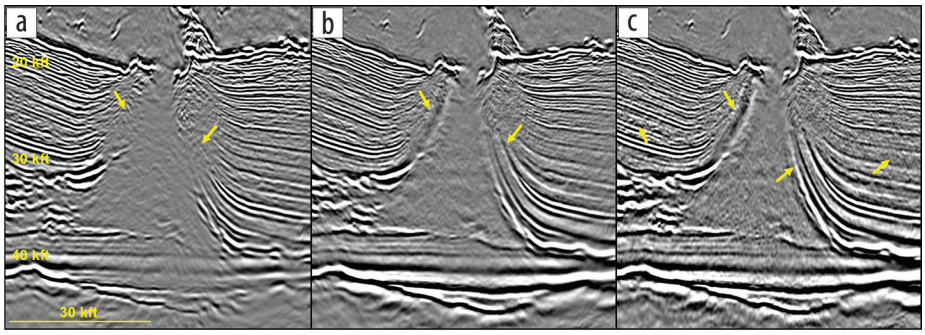

Figure 8. Comparisons of (a) 15 Hz RAZ RTM, (b) 15 Hz OBN RTM with dense nodes only, and (c) 15 Hz OBN RTM with dense and sparse nodes. The additional illumination from the long-offset OBN data provides better steep-dip imaging. The sparse nodes provide further illumination along the feeder flanks, but they also bring increased noise (seen within the basins, within the salt body, and at basement level).

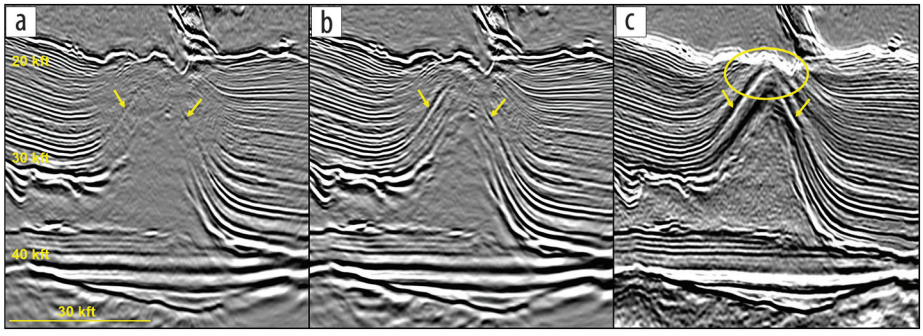

Figure 9. (a) 15 Hz OBN RTM. (b) 15 Hz OBN LSRTM. (c) 15 Hz FWI image. Illumination remains poor even with OBN data, but LSRTM provides some compensation for the weak amplitudes along the steep flanks of the feeder. The best compensation is provided by the FWI image. An estimate of the reflectivity comes directly from the FWI velocity model. The poorly illuminated events (steep dips and basement) show more balanced amplitude, and the steep dips extend all the way to BOS.

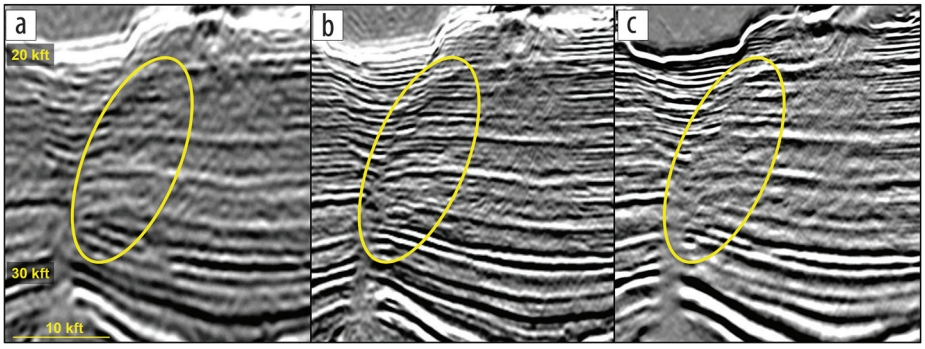

Figure 10. (a) The 11 Hz FWI image already shows the benefits of increased illumination and more balanced amplitudes but lacks resolution. A comparison of (b) the 20 Hz FWI image and (c) the final 25 Hz OBN RTM shows much better imaging of the faults (yellow circles) on the FWI image. They are more continuous with more balanced amplitude and higher S/N. The resolution of the 20 Hz FWI image is comparable to the final 25 Hz OBN RTM.

Seismic interpretation

OBN seismic and FWI image technology are proving to be key enablers to unlock the potential of midlife fields in the subsalt Gulf of Mexico. Subsalt seismic interpretation in the Atwater fold belt is historically difficult due to poor-quality seismic data created by the rugose Sigsbee salt canopy and steep structural flanks of salt stocks. In Shenzi Field, seismic interpretation of particularly challenging areas has relied on supplemental information from well penetrations, reservoir simulations, and history matching to help identify critical faults and stratigraphic features that act as baffles or barriers to fluid flow. Uplift from OBN seismic and FWI images enables higher confidence and more detailed seismic interpretation, providing opportunities to extend the longevity of Shenzi Field. These new technologies have unlocked our subsurface understanding of three key features at Shenzi: (1) fault interpretation of Miocene reservoirs, (2) salt-sediment interactions during Paleogene to Neogene deposition, and (3) structural conformance of amplitudes in largely untested Paleogene reservoirs.

Detailed interpretation of faults and stratigraphic horizons is the backbone to understanding any producing field. The structural

setting at Shenzi includes upturned and faulted strata flanking a centralized salt feeder. Multiple episodes of faulting throughout the Cenozoic, concurrent with a pulse of hydrocarbon migration from the underlying Mesozoic source rocks, set up pockets of oil and gas accumulations in sand-rich Miocene reservoirs. Prior to the OBN survey, seismic interpretation of the legacy 25 Hz dip-enhanced RAZ RTM supported a relatively low density of faults through north-south crosslines in the main producing area of Shenzi Field (Figure 11a). Legacy fault and horizon picks were of relatively low confidence in this challenging region. Seismic interpretation of the 20 Hz FWI image paints a very different picture, with a series of gravity-driven slump faults cutting across stair-stepped Miocene reservoirs and likely detaching in a ductile unit above or near the Oligocene (Figure 11b). Higher-confidence fault interpretations are attributed to better imaging of shallower and deeper sections, where amplitude breaks are largely absent. Large-scale reverse faults through deeper strata are also more clearly imaged and interpreted. Horizon interpretations from the FWI image also show a consistent thinning trend toward the crest, compared to legacy interpretations that have abrupt thickness changes across faults.

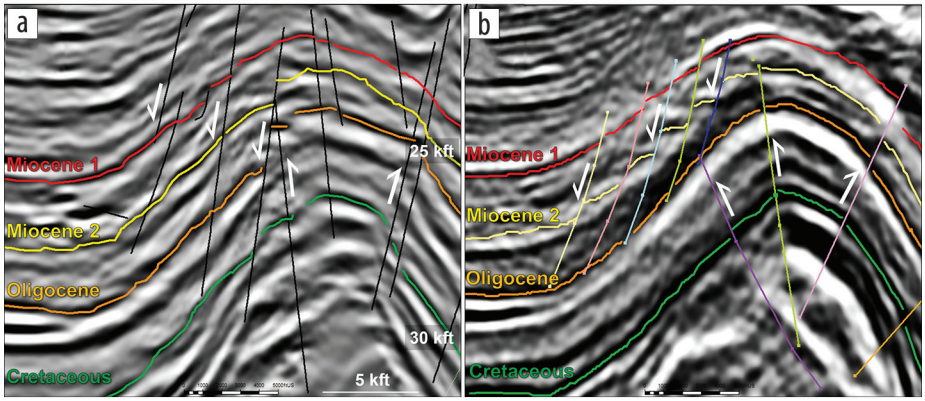

Figure 11. A comparison of the fault interpretation based on (a) the legacy 25 Hz dip-enhanced RTM and (b) the 20 Hz FWI image. High resolution, balanced amplitudes, and good S/N contribute to improving the subsalt image, giving greater confidence to fault picks on the FWI image.

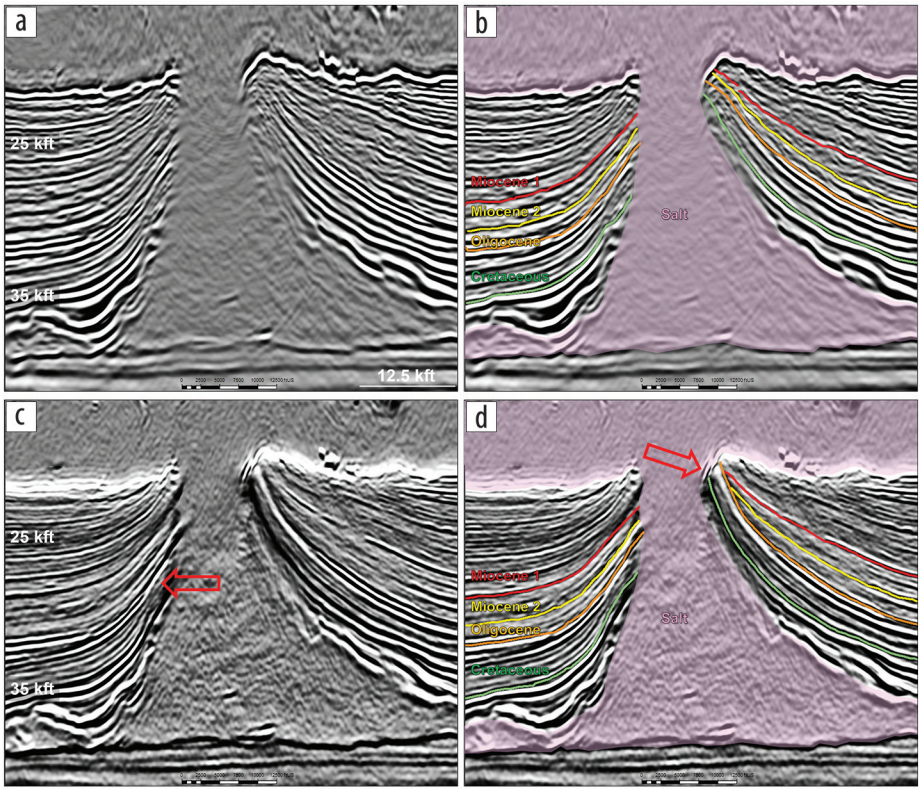

Figure 12. Enhanced 15 Hz RAZ RTM (a) migrated with the final model and (b) with the interpretation overlaid. The same is shown for the 20 Hz FWI image in (c) and (d). The interpretation of the shallow strata east (right) of the feeder has changed substantially. The Paleogene section is upturned and reaching BOS with Miocene layers onlapping (red arrow in d) rather than decreasing in dip near the salt as in (b). In the west (left side of the feeder), an amplitude anomaly (red arrow in c) was observed with early investigations pointing to the possibility of a previously undetected DHI.

On the eastern flank of Shenzi, the relationship between Paleogene and Neogene strata changes drastically with the FWI image interpretation. Interpretation of the 15 Hz RAZ fast track shows strata thinning updip and reaching the crest of the structure, truncated by salt (Figures 12a and 12b). Interpretation of the 20 Hz FWI image upends that geologic scenario by defining a clearly upturned Paleogene section on which Miocene strata onlap downdip of salt (Figures 12c and 12d). This step change in seismic interpretation impacts our understanding of nearly every aspect of the Shenzi petroleum system, including source migration pathways and timing, structural and stratigraphic trapping elements, and reservoir storage and deliverability.

Lastly, seismic uplift on the western flank of Shenzi shows a newly identified amplitude anomaly that conforms to structure in the Paleogene section (Figure 12). Preliminary investigations indicate that the amplitude anomaly is not an illumination artifact, suggesting it could represent a previously undetected large direct hydrocarbon indicator (DHI) in an actively producing field.

Conclusions

In the many years of refining the Shenzi velocity model and interpretation, new technology has always been a disruptor in terms of our understanding of the salt and subsalt structure. This time, recent advances in FWI and an OBN acquisition enabled us to move past the limitations inherent in the existing streamer data set. The sparse node halo added to the core node footprint provided ultra-long offsets that

helped FWI resolve details even beyond the deep autochthonous BOS. Although a more accurate FWI velocity model was the primary expectation from the OBN survey, the long offsets of the OBN also imaged the steep salt flanks for the first time. The sparse nodes proved useful again, contributing to the imaging of these steep salt flanks. Ultimately, the best image of steep dips and faults did not come from the RTM image, but from the image derived directly from the FWI velocity.

Planning for the OBN survey was important to ensure that the acquired data would enable us to meet the imaging objectives. Yet, we also gained new insight from the processing. First, we learned that with the existing streamer survey we could produce a fast-track volume within a month of completing the OBN acquisition, which could provide important imaging uplift and help influence well planning. Reducing cycle time of imaging projects has been a long-standing industry goal. With FWI using OBN data for automatic salt model building, this goal has become reality.

The second lesson learned was that velocity models can never be fully resolved with a manual interpretation workflow. While evaluating our result, we tested several salt scenarios that modified the FWI velocity to better fit our previous understanding of the structure. These changes always made things worse. In comparison, a data-driven approach and its image improvements, from increased focusing and continuity in the shallow subsalt down to a very coherent and rather simple basement structure, together with the different quality controls we conducted, gave much higher confidence in the validity of our final image. Yet, in areas with reduced diving-wave illumination, such as just below BOS, well information was useful to manually guide the FWI solution. Even though the impact of these edits was minor, it shows that an understanding of the limitations of the FWI-driven method is important.

The third lesson learned was that a high-frequency FWI image can compete as the primary interpretation volume. With an FWI frequency of 20 Hz, the subsalt resolution approached that of the final 25 Hz RTM. Its structural benefits, such as coherence of events, especially steep dips and faults, is superior in many places to the RTM. The FWI image becomes a new addition to the imaging and interpreter toolbox. This could become increasingly powerful as more physics is incorporated into the modeling and inversion, such as density, anisotropy, absorption, and elasticity.

The step change achieved in Shenzi imaging was the result of the new technology used in the acquisition and processing. After many years of incremental changes, this is an exciting time to be involved in seismic imaging. TLE

Acknowledgments

We thank BHP and Repsol for permission to publish this work. We thank our BHP colleague Ted Naylor for building the detailed GOCAD model used for the feasibility and survey design. We thank many CGG colleagues for project support and long discussions.

Data and materials availability

Data associated with this research are confidential and cannot be released.

Corresponding author: cheryl.mifflin@bhp.com

References

Ahmed, I., 2018, Diving wave illumination using RTM to analyze acquisition geometries for FWI: 88th Annual International Meeting, SEG, Expanded Abstracts, 1299–1303, https://doi.org/10.1190/segam2018-2997116.1.

Chakraborty, S., E. L'Heureux, K. Hartman, Q. Li, I. Ahmed, C. Joy, A. Brenders, J. P. Sandschaper, and S. Michell, 2017, Thunder Horse ocean-bottom nodes acquisition design: 87th Annual International Meeting, SEG, Expanded Abstracts, 226–231, https://doi.org/10.1190/segam2017-17681262.1.

Howard, M., 2007, Marine seismic surveys with enhanced azimuth coverage: Lessons in survey design and acquisition: The Leading Edge, **26**, no. 4, 480–493, https://doi.org/10.1190/1.2723212.

Kumar, R., H. Zhu, V. Vandrasi, D. Dobesh, and A. Vazquez, 2019, Updating salt model using FWI on WAZ data in the Perdido area: Benefits and challenges: 89th Annual International Meeting, SEG, Expanded Abstracts, 1270–1274, https://doi.org/10.1190/segam2019-3216761.1.

Mei, J., Z. Zhang, F. Lin, R. Huang, P. Wang, and C. Mifflin, 2019, Sparse nodes for velocity: Learnings from Atlantis OBN full-waveform inversion test: 89th Annual International Meeting, SEG, Expanded Abstracts, 167–171, https://doi.org/10.1190/segam2019-3215208.1.

Michell, S., X. Shen, A. Brenders, J. Dellinger, I. Ahmed, and K. Fu, 2017, Automatic velocity model building with complex salt: Can computers finally do an interpreter's job?: 87th Annual International Meeting, SEG, Expanded Abstracts, 5250–5254, https://doi.org/10.1190/segam2017-17778443.1.

Nolte, B., F. Rollins, Q. Li, S. Dadi, S. Yang, J. Mei, and R. Huang, 2019, Salt velocity model building with FWI on OBN data: Example from Mad Dog, Gulf of Mexico: 89th Annual International Meeting, SEG, Expanded Abstracts, 1275–1279, https://doi.org/10.1190/segam2019-3216777.1.

Shen, X., I. Ahmed, A. Brenders, J. Dellinger, J. Etgen, and S. Michell, 2018, Full-waveform inversion: The next leap forward in subsalt imaging: The Leading Edge, **37**, no. 1, 67b1–67b6, https://doi.org/10.1190/tle37010067b1.1.

van Gestel, J.-P., E. L'Heureux, J. R. Sandschaper, P.-O. Ariston, N. D. Bassett, and S. Dadi, 2015, Atlantis "beyond 4D" ocean bottom nodes acquisition design: 85th Annual International Meeting, SEG, Expanded Abstracts, 125–129, https://doi.org/10.1190/segam2015-5847522.1.

Wang, P., A. Gomes, Z. Zhang, and M. Wang, 2016, Least-squares RTM: Reality and possibilities for subsalt imaging: 86th Annual International Meeting, SEG, Expanded Abstracts, 4204–4209, https://doi.org/10.1190/segam2016-13867926.1.

Wang, P., Z. Zhang, J. Mei, F. Lin, and R. Huang, 2019, Full-waveform inversion for salt: A coming of age: The Leading Edge, **38**, no. 3, 204–213, https://doi.org/10.1190/tle38030204.1.

Xue, Z., Z. Zhang, F. Lin, J. Mei, R. Huang, and P. Wang, 2020, Full-waveform inversion for sparse OBN data: 90th Annual International Meeting, SEG, Expanded Abstracts, 686–690, https://doi.org/10.1190/segam2020-3427891.1.

Zhang, Z., J. Mei, F. Lin, R. Huang, and P. Wang, 2018, Correcting for salt misinterpretation with full-waveform inversion: 88th Annual International Meeting, SEG, Expanded Abstracts, 1143–1147, https://doi.org/10.1190/segam2018-2997711.1.

Zhang, Z., Z. Wu, Z. Wei, J. Mei, R. Huang, and P. Wang, 2020, FWI imaging: Full-wavefield imaging through full-waveform inversion: 90th Annual International Meeting, SEG, Expanded Abstracts, 656–660, https://doi.org/10.1190/segam2020-3427858.1.